Materialia 24 (2022) 101497

Contents lists available at ScienceDirect

Materialia

journal homepage: www.elsevier.com/locate/mtla

Diffusion of multi-principal elements through stable Cr_2O_3 and Al_2O_3 scales

Indranil Roy[a], Pratik K. Ray[b], Ganesh Balasubramanian[a,*]

[a] Mechanical Engineering and Mechanics, Lehigh University, Bethlehem, PA 18015, USA
[b] Metallurgical and Materials Engineering, Indian Institute of Technology Ropar, Rupnagar, Punjab 140001, India

ARTICLE INFO

Keywords:
High entropy alloy
Oxidation
Diffusion coefficient
Molecular dynamics
Nudge elastic band
Migration energy
Tracer diffusion

ABSTRACT

Understanding the oxidation mechanisms in multi-principal elements and high-entropy alloys (HEAs) is critical for their potential applications in high-temperature oxidative environmnts. In addition to the compositional complexity, the counter-diffusion of cations and anions through the oxide contributes to the growth of the oxide scales in these materials. We examine the cationic and anionic diffusion through the stable chromium and aluminum oxides that form in a model HEA using atomistic simulations. In accord with experiments, we find that the tracer cations diffuse faster than the native cations through the oxide scales at high temperature (1000 K to 2000 K) and the dynamics are directly correlated to the respective migration energies of the diffusion pathways. The oxide scale growth is strongly influenced by the presence of tracer/impurity elements in alumina forming alloys relative to those that predominantly form chromia. A geometric analysis of the vacancy-induced diffusion paths for the cation migration relative to the location of the oxygen atoms reveals the influence of the latter on the preferential diffusion pathway, resulting in anisotropy. The predictions offer insights on the diffusion characteristics in the oxide scales formed in HEAs and aid in our understanding of the oxide growth kinetics.

1. Introduction

High-entropy alloys (HEAs) have attracted significant interest as potential candidates for high temperature applications [1]. While the structural characteristics of these materials have been extensively examined [2], literature on their oxidation resistance is limited. Understanding, predicting and improving the oxidation resistance of these alloys is a significant challenge that needs to be addressed if these materials are to be used in high temperature oxidative environments such as in gas turbines, in hypersonic vehicles, to cite a few. The complexity of this challenge arises from the presence of multiple chemical species, whose role in modifying the oxidation resistance is not yet well-understood [3]. For successful modeling of oxidation in an HEA, it is of interest to quantitatively understand diffusion through each oxide. Experimental reports on diffusion coefficient values are inconsistent and rare [4,5]. Atomistic modeling tools [6,7] such as molecular dynamics can calculate consistent and repeatable diffusion coefficient values that can be adopted for mesocale oxidation modeling [8]. The growth of an oxide layer is contingent on the counter-diffusion of cations and anions through the oxide. Here, we focus on modeling the diffusivities of various species through the chromia and alumina scale, which happen to be the oxide scales that form during steady state oxidation of Al and Cr containing HEAs, which are one of the the most widely reported HEA in the literature. We approach the problem from an atomistic perspective by using Molecular Dynamics (MD) simulations coupled with the Nudged Elastic Band method (NEB) [9] calculations. Furthermore, we also assess the diffusion pathways and elucidate the role that various transition metals might play during the oxidation process. We expect that the diffusivities, once evaluated through this work, may be coupled with mesoscale models [8] for quantitative prediction of the oxidation kinetics.

Self-diffusion of anions and cations through various oxides have been well-established for a number of oxides such as Cr_2O_3 [10]. However, relatively few tracer-diffusion simulations and experiments have been performed that are relevant for understanding the oxidation of HEAs. We attempt to address this lacuna by interrogating the diffusivities through potential oxide scales for an equiatomic AlFeCoCrNi HEA. Prior experimental efforts have indicated that the external oxide scale consists of alumina and chromia [11]. However, other transition elements may also be present in these scales, especially during the initial transient oxidation phase. We employ MD simulations for studying the tracer diffusion behavior of multiple cations through alumina and chromia. The elements considered include iron (Fe), nickel (Ni) and cobalt (Co), in addition to Al and Cr with the goal of predicting a set of diffusion coefficients necessary for modeling the oxidation behavior of AlFeCoCrNi HEA. The MD simulations aid in describing the temperature dependent diffusivities of all the elements when present individually in the alumina and chromia scales, while NEB calculations are used for estimating the minimum energy paths for diffusion.

* Corresponding author.
E-mail address: gab317@lehigh.edu (G. Balasubramanian).

https://doi.org/10.1016/j.mtla.2022.101497
Received 15 March 2022; Accepted 28 June 2022
Available online 1 July 2022

2. Computational methods

Both $\alpha - Cr_2O_3$ and $\alpha - Al_2O_3$ assume the corundum structure of hexagonal unit cell [12,13]. For the vacancy mediated diffusion coefficient calculation, we construct $18 \times 18 \times 18$ supercell containing 58,320 atoms with periodic boundary conditions. To calculate the diffusion coefficients of tracer elements, viz., Fe, Ni, Co and Al/ Cr through $\alpha - Cr_2O_3$ and $\alpha - Al_2O_3$, we randomly replace Cr/Al cation sites in oxides with one type of tracer element. The results reported here are for 0.08% vacancy and 10% tracer element concentration; nonetheless, the findings are independent of these concentration variations. All the elements assume their normal charges. We use the highly-parallelized Large-scale Atomistic Molecular Massively Parallelized Simulator (LAMMPS) [14] for all our simulations. For modeling the pure oxides, we adopt the short-ranged Buckingham potential [15] in combination with the long-ranged Coulombic term. The cut-off distance for both the long- and short-ranged interactions is 10Å. For the oxides, the Buckingham potentials are well established in terms of reliability [12,13,16–20]. The self-interactions of tracer elements and the cross-interactions with the oxide are described using the 12/6 Lennard–Jones (LJ) potential [21]. The LJ-potential parameters for the cross-interactions are estimated using the Lorentz–Berthelot mixing rule as $\epsilon_{ij} = (\epsilon_i \epsilon_j)^{1/2}$ and $\sigma_{ij} = (\sigma_i + \sigma_j)/2$, where i and j are two representative elements, σ is the effective distance between two atoms when the repulsion is extreme, and ϵ is the depth of the potential well. The parameters for all the potentials employed are listed in Table 1. For calculating diffusion coefficient at different temperatures, system is equilibrated in NPT (isobaric-isothermal) and NVT (canonical) ensemble before performing Mean Square Displacement (MSD) calculations. The diffusion coefficient is the slope of the MSD curves.

The Nudged Elastic Band (NEB) [9] simulations are performed to calculate the migration energy of vacancy induced diffusion. In a supercell that contains 480 atoms, five different cation sites are selected at different distances from the vacancy (Table 2). Among the five possible migration paths considered, three in *ab*-plane and two in *c*-plane are the nearest neighbors of a cation vacancy that represents all the atoms in the two planes (Fig. 2(a)).

Table 1
Parameters employed for the Buckingham and Lennard–Jones interatomic potentials.

Potential Type	Interaction	A (eV)	r (Å)	Reference
Buckingham	Cr^{+3} - O^{-2}	1204.18	0.3165	[22]
Buckingham	Al^{+3} - O^{-2}	3411.118	0.244549	[23]
Buckingham	O^{-2} - O^{-2}	9547.96	0.21916	[24]
Potential Type	**Atom Type**	ϵ	σ	**Reference**
Lennard–Jones	Al	0.392	2.260	[25]
Lennard–Jones	Cr	0.502	2.336	[25]
Lennard–Jones	Co	0.510	2.306	[25]
Lennard–Jones	Fe	0.527	2.321	[26]
Lennard–Jones	Ni	0.520	2.282	[26]
Lennard–Jones	O	0.0047	3.289	[27]

Table 2
The migration energy of different elements during hops from multiple locations into Cr vacancy are listed. The migration energy for element i is given by E_m^i in eV. The last three parameters are the distance of the vacancy from respective atom positions in *ab*-plane (d_{ab}), *c*-plane (d_c) and the normal distance d in Å.

Path	E_m^{Cr}	E_m^{Al}	E_m^{Fe}	E_m^{Co}	E_m^{Ni}	d_{ab} (Å)	d_c (Å)	d (Å)
1	0.971	1.305	1.325	1.325	1.537	2.84	0.385	2.865
2	8.188	6.295	5.225	5.225	4.371	4.95	0	4.95
3	7.86	6.54	5.012	5.012	4.785	5.73	0.385	5.74
4	2.668	1.44	1.542	1.542	1.602	0	2.65	2.65
5	1.107	0	0.012	0.012	0.048	0	4.145	4.145

For statistical consistency, we have repeated the simulations for ease case at least four times. Note that we have two types of activation energies, i.e., (1) the bulk activation energy for diffusion (Q) [kJ/mol], and (2) the migration energy for an atom to jump into a vacancy (E_m) [eV/atom]. As the energy in the second case is expected to be very small, the unit is in terms of eV (per migrating atom). To the best of our knowledge, comparison between these two activation energies for alumina and chromia has not been reported in the literature. With a view to connect the two energy quantities, we convert the kJ/mol unit into eV/atom and compare the results below. The unit conversion is performed as: Unit [Q] = $\frac{\text{kJ}}{\text{mol}} = \frac{\text{kJ}}{6.023\times10^{23}\ \text{molecules Cr}_2\text{O}_3} = \frac{6.242\times10^{21}\ \text{eV}}{6.023\times10^{23}\ \text{molecules Cr}_2\text{O}_3} = \frac{1.036\times10^{-2}\ \text{eV}}{\frac{2}{5}\ \text{Cr atoms}} = 2.59\times10^{-2}\ \frac{\text{eV}}{\text{Cr atom}} = 2.59\times10^{-2} \times \text{Unit}[E]$.

3. Results and discussion

We calculate vacancy mediated diffusion coefficient of Cr and O in the chromia crystal in the temperature range of 800 K to 2000 K. The results are in agreement with the previous computational reports [12,13,28]. The variation of diffusion coefficient with temperature follows an Arrhenius relationship, as shown in Fig. 1(a). Our simulations suggest minimal variation in diffusion coefficients with vacancy concentration, consistent with the literature. The O anion diffuses faster than the Cr cation at high temperatures, while diffusion of Cr dominates at lower temperatures. The high temperature simulations are performed to verify the predictions of our computational methods against earlier studies. The chromia scale suffers from poor stability at temperatures above ~1250 K due to volatilization [29]. It has been observed experimentally that chromia scales are stable at the lower temperature regimes, where the cation diffusion is faster than anion diffusion resulting in a net outward growth of the oxide scale, in concurrence with the findings from our simulations. We note that the activation energy (Q) for O (88.3403 kJ/mol) is almost twice that for Cr (44.49 kJ/mol) while the pre-exponential factor is two orders of magnitude higher for O than Cr; these results indicate that the O diffusion coefficient has a stronger temperature dependence. Protective Cr_2O_3 scale forms primarily through outward cation (Cr^{+3}) diffusion that is predominant at low temperatures (< 1250 K). Therefore, the low activation energy of Cr helps in the formation of stable Cr_2O_3 scale below 1250 K and prevents catastrophic degradation by oxidation in Cr containing alloys.

The diffusion coefficients of select cations (Al, Cr, Fe, Co, Ni) are investigated by implanting them as tracer elements in both chromia and alumina scales. The simulations are performed by varying the tracer element concentration and we ascertain that the diffusion coefficients do not vary with compositions. We find that the diffusion coefficients follow an Arrhenius relationship over the temperature range under consideration (i.e., 1000 K to 2000 K). Similar to the previous case, faster diffusing parent element changes from Cr to O after reaching a particular temperature for all tracer element additions except for Ni-doped Cr_2O_3 (Fig. 1(e)). Presence of Ni results in a lower activation energy for O diffusion (46.8842 kJ/ mol) relative to the undoped oxide and becomes almost equal to that of Cr (44.323 kJ/ mol). Activation energies being nearly identical, the relative diffusivities are dominated by the difference in the pre-exponential term, which suggests that Ni additions can promote the inward diffusion of O. The activation energy for Ni diffusion is also comparatively low (55.50 kJ/mol) among all the tracer elements investigated here, which indicates the possibility of Ni-oxide forming along with chromia. The diffusion coefficient of all tracer elements over the temperature range investigated is almost always higher than both Cr and O. Among the individual tracers, Al diffuses fastest at lower temperatures, while Fe and Co are the slowest. The activation energy of Al (47.93 kJ/mol) is almost equal to that of Cr (46.96 kJ/mol). At higher temperatures, Fe and Co diffuse more rapidly that both Al and Ni. Interestingly, the temperature dependence of the diffusion profiles for both Fe- and Co-doped chromia are similar. The activation energy of

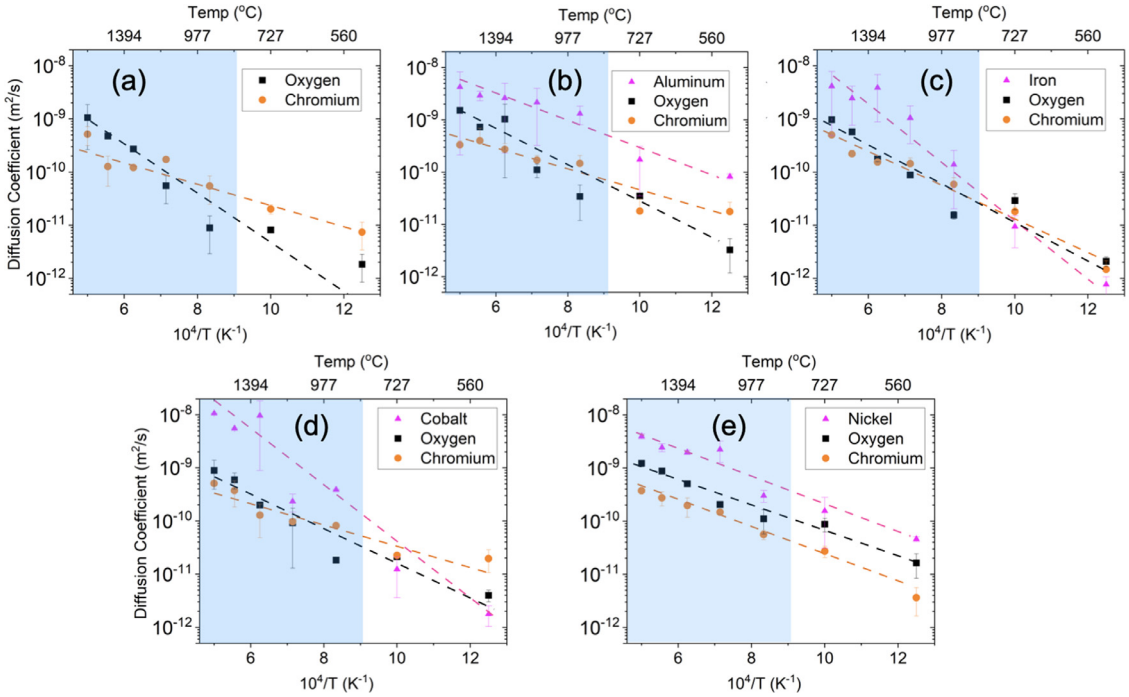

Fig. 1. Arrhenius plot of diffusion coefficient variation with temperature in chromia. The variation of diffusion coefficients in (a) pure Cr_2O_3 (a) and with doping of tracer element, viz., (b) Al, (c) Fe, (d) Co and (e) Ni, are presented on logarithmic scale. The shaded region denotes the high temperature zone where Cr_2O_3 is unstable [29].

Fe and Co are 103.08 and 112.10 kJ/mol, respectively, while the pre-exponential factor is highest for Co (1.27×10^{-5} cm^2/s) amongst all the elements.

For an atom to migrate from one position to another through a particular path, it needs to overcome a minimum energy barrier, i.e., the migration energy. To understand the diffusion of different elements in the oxide scale, we calculate migration energy for five possible hopping paths of a cation leading to a Cr vacancy. The migration energy variation for Cr jump (Fig. 2(b)) concurs with the report of Cao et al. [13] and the same for Fe and Ni migration is consistent with the density functional theory based NEB report by Rak et al. [28], which are the only two reports on chromia to the best of our knowledge.

As discussed above with regards to the diffusion coefficient plots (Fig. 1), diffusion characteristics of Fe and Co are similar, also inferred from Fig. 2(d) and (e). Fe and Co have near-identical behavior of migration energy change during hopping through the different paths. For Cr to migrate into a Cr vacancy, path 1 is the easiest as it has lowest migration (0.971 eV) energy, followed by path 5 (1.107 eV). When a tracer element is added for hopping, the lowest energy path is 5. Path 5 has the lowest migration energy for all the tracer elements, which indicates that diffusion through chromia is most likely anisotropic. This prediction is in agreement with previously reported results [13]. The activation energy values for migration through different paths are listed in Table 2. Al diffuses fastest through path 5 among all the elements considered here. Some of the energy barriers as a function of distance are multi-mounted (Fig. 2) because when migrating from the original position to the vacancy, the cation has to pass through multiple layers of anions. Paths 2 and 3 (both in *ab*-plane) has considerably high activation energy for all the elements compared to the other paths. Therefore, an atom will very rarely take any of these paths during migration.

The comparison of migration energies (E_m) from NEB with activation energies of the bulk (Q) from the diffusion coefficient shows that both are of the same order. In fact, Q_{Cr} in pure Cr_2O_3 is 1.1524 $\frac{eV}{Cr\ atom}$ which is just above the E_{Cr} of the minimum energy path (MEP) (0.971 eV). While multiple diffusion pathways do exist in the crystal, one anticipates that the cations will have a higher probability of diffusion through the low migration energy paths and the overall activation energy observed in our MD simulations is essentially weighted average over all possible paths. Further discussion on the comparison between migration energy from NEB and bulk activation energy from diffusion coefficient calculation needs to be based on expensive NEB simulation which is not in the scope of this work.

The tracer cations diffuse faster than the native cation in the Al_2O_3 scale (Fig. 3), which is consistent to our observations in Cr_2O_3. The experimental reports of diffusion coefficients in the literature vary by orders of magnitude depending on the type of diffusion measurement (intrinsic or extrinsic), crystallinity (single phase, polycrystalline) and technique used (diffusion couple or isotope exchange) [30]. Here, we focus primarily on lattice diffusion. We find that the diffusion coefficient of Al and O is near-identical at low temperature, while O diffuses slightly faster towards higher temperature range. It is interesting to note that unlike Cr_2O_3, the Al_2O_3 scale is primarily formed by downward diffusing O^{-2} anions. Again, compared to chromia, the diffusion coefficient of Al and O are one order of magnitude higher in alumina. The switching of faster diffusing species (from cation to anion) at elevated temperatures is not as significant in alumina as it is for chromia. The activation energy for diffusion of Al and O are very similar, e.g., 26.62 kJ/mol for Al and 28.42 kJ/mol for O. This trend is consistent for pre-exponential factors as well. These values are considerably low compared to that for the chromia scale. In presence of tracer elements, this behavior is retained while the diffusion coefficients of the tracer elements are almost two orders of magnitude higher than the native elements. An interesting anomaly that is observed between Al-doped Cr_2O_3 and Cr-doped Al_2O_3 is the difference of activation energies of O. For both the cases, the activation energy of cations (Al^{+3} and Cr^{+3}) are comparable, while O has a higher activation energy in Cr_2O_3 (70.89 kJ/mol) than in Al_2O_3 (24.25 kJ/mol). We conjecture that this result is indicative of a mixed $(Al, Cr)_2O_3$ scale formation that would also proceed via predominantly the outward cationic diffusion [31]. The low activation energy of O in Al_2O_3 helps anions to penetrate easier through the scale which results in inward growth of ox-

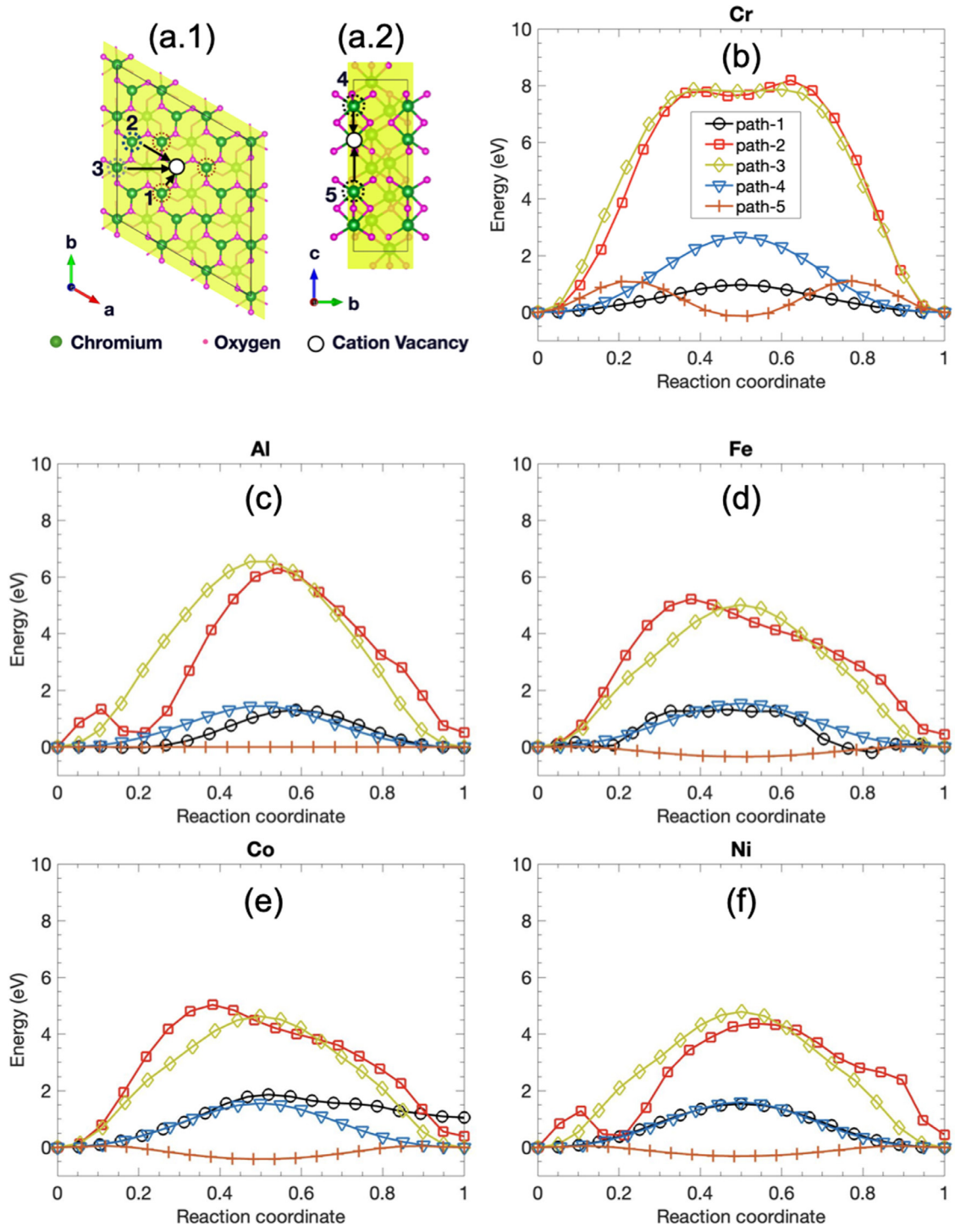

Fig. 2. Migration energies for cation hopping into a Cr vacancy obtained from the Nudged Elastic Band (NEB) method. Three among the five possible paths for the hop are in (a.1) *ab* plane and two are in (a.2) *c*-plane. The variation of vacancy induced migration energy for pure (b) Cr and that doped by the four tracer elements, viz., (c) Al, (d) Fe, (e) Co and (f) Ni are presented on a logarithmic scale.

ide; the opposite occurs for Cr_2O_3 formation i.e., Cr^{+3} diffuses upward as O has a high activation energy barrier to overcome. Our simulation outcomes on pure oxides also support this argument. O^{-2} has twice the activation energy of Cr^{+3} in Cr_2O_3 (88 versus 44 kJ/mol, respectively) while O^{-2} and Al^{+3} have comparable activation energies in Al_2O_3 (28 and 26 kJ/mol, respectively). These predictions corroborate the ease of O diffusion in Al_2O_3 than in the Cr_2O_3 scale.

A comparison of the diffusion coefficients of Cr doped Al_2O_3 against Al doped Cr_2O_3 reveals an exciting insight. The diffusion coefficient of Cr in Al_2O_3 is higher than Al in Cr_2O_3 at all temperatures. The higher diffusion coefficient implies that Cr moves faster and will situate on top of the Al_2O_3 layer. Previous experimental literature on the AlCoCrFeNi system have shown an external chromia layer followed by an internal alumina [32] formation. The pre-exponential factors of O^{-2} and Cr^{+3} in Al_2O_3 are of the same order, while O^{-2} has two orders of magnitude higher pre-exponential factor than Cr^{+3} in Al_2O_3. This difference implies the frequent longer distance jumps of O^{-2} in the Cr_2O_3 scale. Ni has the highest activation energy of 32.45 kJ/mol while all other elements

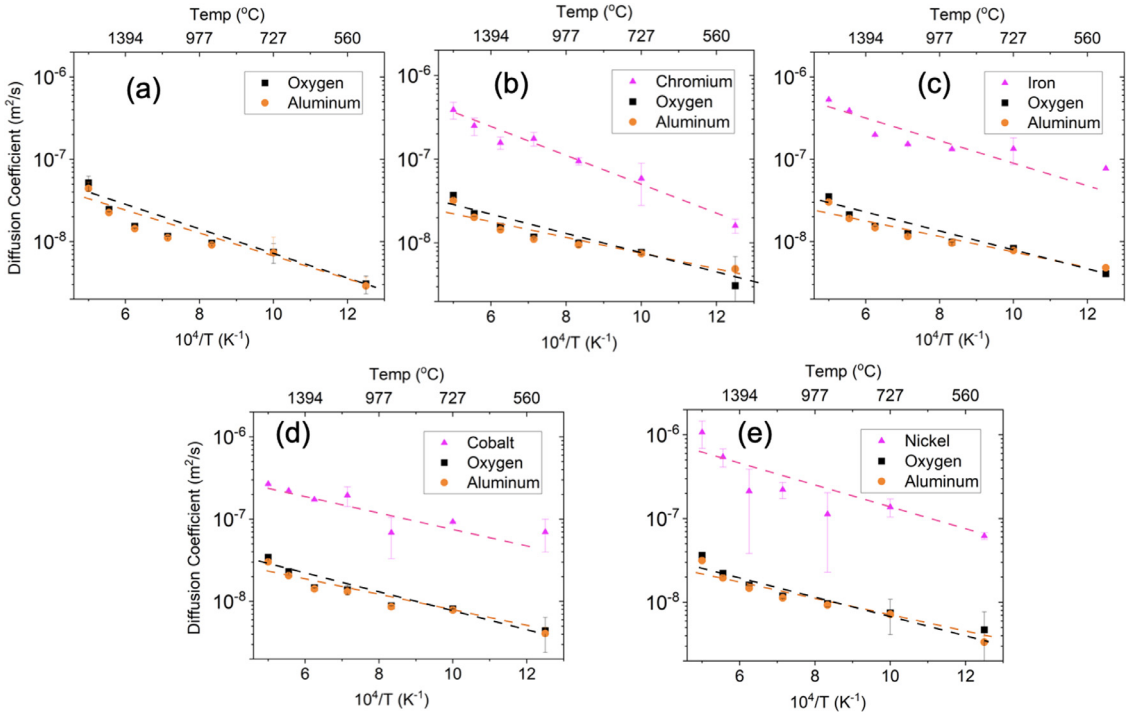

Fig. 3. Arrhenius plot of diffusion coefficient variation with temperature in alumina. The variation of diffusion in (a) pure Al_2O_3 and with doping of tracer elements, viz., (b) Cr, (c) Fe, (d) Co and (e) Ni are presented.

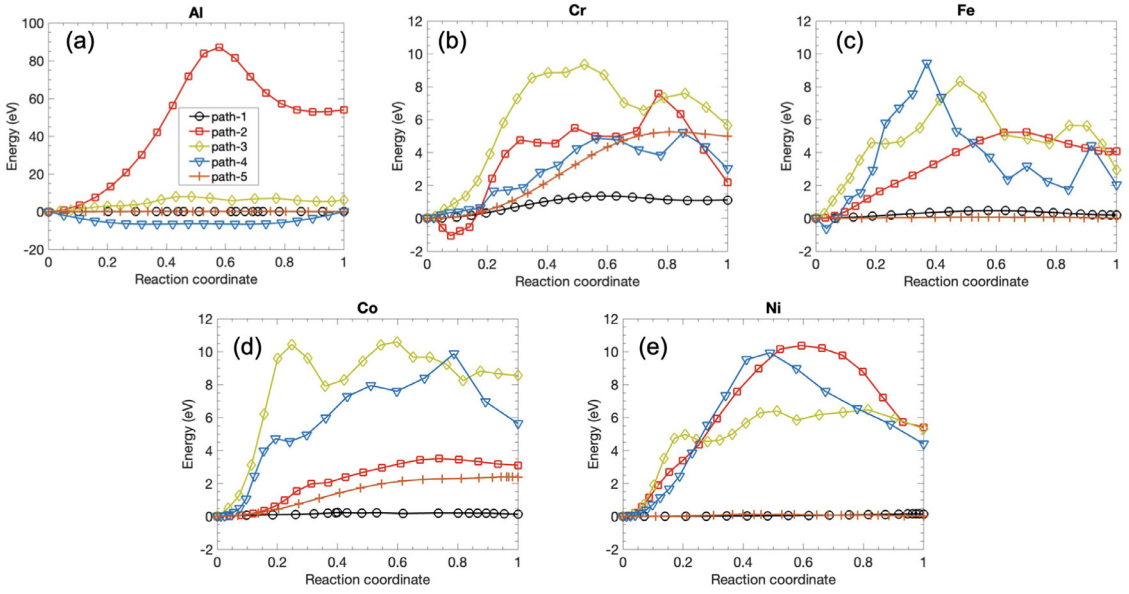

Fig. 4. Migration energies for cation hopping into a Al vacancy is obtained from the Nudged Elastic Band (NEB) method. The variation of vacancy induced migration energy of (a) Al and with the doping of the four tracer elements, viz., (b) Cr, (c) Fe, (d) Co and (e) Ni are presented.

(including O and Al) have Q varying between 18–22 kJ/mol. Unlike in chromia, Ni addition does not result in switching of the oxidation mechanisms in the Al_2O_3 scale.

The variation of migration energy with reaction coordinates for vacancy mediated diffusion of different elements through alumina are presented in Fig. 4 and the migration energies thorough the five paths are listed in Table 3. As no saddle point can be located for Cr diffusion through path 5 (Fig. 4), no activation energy is defined for that particular case. The vacancy mediated migration energy for Al is lowest through path 4 (≈ 0 eV). As evident from the plots (b-e), the migrated tracer atoms are unstable at the vacancy because the energy does not reach zero, possibly implying that the atoms will reside in the vacancy for a short duration before returning to a different lower energy position. This phenomenon also occurs for the interstitial diffusion of Fe and Ni in Cr_2O_3 as reported by Rak *et al* [28]. There are multiple saddle points for Path 2, 3 and 4 which indicate that the atoms are stable at the interim site. Among tracer elements, Path 1 is favored by Cr and Co while Ni and Fe have the lowest energy barrier though Path 5. For Al diffusion, the Path 2 has its saddle point at 87.2 eV, indicating a very high energy barrier. Therefore, Path 2 will be very rarely adopted for diffusion. The timestep required for migration energy simulations of alumina is two orders of magnitude smaller than the same set of simulations for chromia.

Table 3
Migration energy of different elements during hops from multiple locations into Al vacancy. The migration energy of element i for hop is given by E_m^i in eV units. The last three parameters are the distance of vacancy from respective atom positions in ab-plane (d_{ab}), c-plane (d_c) and the normal distance d in Åunits.

Path	E_m^{Al}	E_m^{Cr}	E_m^{Fe}	E_m^{Co}	E_m^{Ni}	d_{ab} (Å)	d_c (Å)	d (Å)
1	0.163	1.358	0.464	0.229	0.149	2.84	0.385	2.86
2	87.198	7.591	5.242	3.508	10.374	4.95	0	4.95
3	8.007	9.359	8.332	10.588	6.473	5.73	0.385	5.74
4	0.001	5.213	9.451	9.88	9.938	0	2.65	2.65
5	0.202	–	0.069	2.403	0.126	0	4.145	4.145

As discussed earlier in the case of chromia, a comparison of the migration energy of a single atom (E_m) with the activation energy of the bulk diffusion (Q) can be reproduced for the case of Al_2O_3. The value of Q is ~ 0.5 eV that is close to the migration energy values though the minimum energy path (MEP) listed in Table 3. This result is expected as the Q for bulk diffusion must be in the neighborhood, but higher, than the activation energy of migration through the MEP.

We further examine the reason for preferential migration through Paths 1 and 5. Careful scrutiny of the neighbors around a vacancy and location of O^{-2} atom near the migration path (e.g., a line connecting the migrating atom and the vacancy) provides interesting geometric inferences. If a triangle is drawn with the vertices being the (1) vacancy, (2) migrating atom and (3) nearest O^{-2} to the path, the greater the angle at O^{-2} atom vertex, the closer is O^{-2} to the path. As an extreme case, if the angle is 180° at the O^{-2} site, the O^{-2} is directly on the path of migration. We analyze the angles at the O^{-2} vertex for all five paths and find the angle to be smallest for Paths 1 and 5, i.e., $90 \pm 2°$, signifying minimal obstruction during migration. For the other three paths, oxygen occludes the migrating cation as the angle is higher than 120°.

4. Conclusion

The predictions from our simulations lead us to conclude that tracer cations in the oxide tend to diffuse faster than the native cations at high temperature (1000 K to 2000 K). This effect is much more pronounced in alumina as compared to chromia. It appears that this behavior is strongly correlated to migration energies associated with the diffusion pathways in the two different oxides. The differences in migration energy barriers for tracer element cations and the Cr cation are relatively less when compared with the differences in migration energy barriers for tracer element cations and the Al cation. This result indicates that the oxide scale growth will be strongly influenced by the presence of tracer/impurity elements in alumina forming alloys relative to that in chromia forming alloys. Oxidation of compositionally complex alloys result in complex scales with multiple impurity cations present in addition to host cations. It is expected that a migration energy based assessment of diffusion pathways in host oxides, as presented here, can guide alloy design in part by providing insights on the diffusion characteristics in the oxide scale, which is in turn related to the scale growth kinetics.

Data availability

The authors declare that the data supporting the findings of this study are available from the corresponding author upon reasonable request.

Declaration of Competing Interest

The authors declare that they have no known competing financial interests or personal relationships that could have appeared to influence the work reported in this paper.

CRediT authorship contribution statement

Indranil Roy: Investigation, Formal analysis, Writing – original draft, Writing – review & editing. **Pratik K. Ray:** Conceptualization, Supervision, Formal analysis, Writing – original draft, Writing – review & editing. **Ganesh Balasubramanian:** Funding acquisition, Supervision, Resources, Writing – review & editing.

Acknowledgments

The work was supported in part by the National Science Foundation (NSF) through award CMMI-1944040. The simulations were performed on the Lehigh University LTS computing cluster, Hawk, acquired through the NSF award OAC-2019035.

References

[1] S. Praveen, H.S. Kim, High-entropy alloys: potential candidates for high-temperature applications–an overview, Adv. Eng. Mater. 20 (1) (2018) 1700645.
[2] E.P. George, W. Curtin, C.C. Tasan, High entropy alloys: a focused review of mechanical properties and deformation mechanisms, Acta Mater. 188 (2020) 435–474.
[3] F. Gesmundo, B. Gleeson, Oxidation of multicomponent two-phase alloys, Oxid. Met. 44 (1) (1995) 211–237.
[4] Y. Oishi, W. Kingery, Self-diffusion of oxygen in single crystal and polycrystalline aluminum oxide, J. Chem. Phys. 33 (2) (1960) 480–486.
[5] A.E. Paladino, W. Kingery, Aluminum ion diffusion in aluminum oxide, J. Chem. Phys. 37 (5) (1962) 957–962.
[6] Y.-Z. Wang, Y.-J. Wang, Disentangling diffusion heterogeneity in high-entropy alloys, Acta Mater. 224 (2022) 117527.
[7] T. Shi, Z. Su, J. Li, C. Liu, J. Yang, X. He, D. Yun, Q. Peng, C. Lu, Distinct point defect behaviours in body-centered cubic medium-entropy alloy NbZrTi induced by severe lattice distortion, Acta Mater. 229 (2022) 117806.
[8] I. Roy, P.K. Ray, G. Balasubramanian, Examining oxidation in β-NiAl and β-NiAl + Hf alloys by stochastic cellular automata simulations, npj Mater. Degrad. 5 (1) (2021) 1–9.
[9] G. Henkelman, B.P. Uberuaga, H. Jónsson, A climbing image nudged elastic band method for finding saddle points and minimum energy paths, J. Chem. Phys. 113 (22) (2000) 9901–9904.
[10] P. Cao, D. Wells, M.P. Short, Anisotropic ion diffusion in α-Cr_2O_3: an atomistic simulation study, Phys. Chem. Chem. Phys. 19 (21) (2017) 13658–13663.
[11] A. Anupam, A.S. Ang, K. Guruvidyathri, M. Abbas, D. Sivaprahasam, P. Munroe, C. Berndt, B. Murty, R.S. Kottada, Evaluating the influence of microstructural attributes: fraction, composition, size and spatial distribution of phases on the oxidation behaviour of high-entropy alloys, Corros. Sci. 184 (2021) 109381.
[12] Molecular dynamics simulations of vacancy diffusion in chromium (III) oxide, hematite, magnetite and chromite, Solid State Ionics 270 (2015) 10–17.
[13] P. Cao, D. Wells, M.P. Short, Anisotropic ion diffusion in Cr_2O_3: an atomistic simulation study, Phys. Chem. Chem. Phys. 19 (2017) 13658–13663.
[14] S. Plimpton, Fast parallel algorithms for short-range molecular dynamics, J. Comput. Phys. 117 (1) (1995) 1–19.
[15] A.E. Ismail, M. Tsige, P.J. Veld In't, G.S. Grest, Surface tension of normal and branched alkanes, Mol. Phys. 105 (23–24) (2007) 3155–3163.
[16] J. Wang, D. Shin, S. Shin, Comprehensive evaluation and parametric sensitivity of interatomic potential models for diffusion kinetics of Cr_2O_3 in molecular dynamics, AIP Adv. 9 (1) (2019) 015123.
[17] L. Minervini, R.W. Grimes, J.A. Kilner, K.E. Sickafus, Oxygen migration in lanio, J. Mater. Chem. 10 (2000) 2349–2354.
[18] L. Minervini, M.O. Zacate, R.W. Grimes, Defect cluster formation in M_2O_3-doped CeO_2, Solid State Ionics 116 (3-4) (1999) 339–349.
[19] R.W. Grimes, D.J. Binks, A.B. Lidiard, The extent of zinc oxide solution in zinc chromate spinel, Philos. Mag. A 72 (3) (1995) 651–668.
[20] A. Chroneos, D. Parfitt, J.A. Kilner, R.W. Grimes, Anisotropic oxygen diffusion in tetragonal $La_2NiO_{4+\delta}$: molecular dynamics calculations, J. Mater. Chem. 20 (2010) 266–270.

[21] D. Wolf, P. Keblinski, S. Phillpot, J. Eggebrecht, Exact method for the simulation of coulombic systems by spherically truncated, pairwise r^{-1} summation, J. Chem. Phys. 110 (17) (1999) 8254–8282.
[22] G. Lewis, C. Catlow, Potential models for ionic oxides, J. Phys. C 18 (6) (1985) 1149.
[23] J. Sun, T. Stirner, W. Hagston, A. Leyland, A. Matthews, A simple transferable interatomic potential model for binary oxides applied to bulk α-Al_2O_3 and the (0 0 0 1) α-Al_2O_3 surface, J. Cryst. Growth 290 (1) (2006) 235–240.
[24] L. Minervini, M.O. Zacate, R.W. Grimes, Defect cluster formation in M_2O_3-doped CeO_2, Solid State Ionics 116 (3–4) (1999) 339–349.
[25] A. Sharma, P. Singh, D.D. Johnson, P.K. Liaw, G. Balasubramanian, Atomistic clustering-ordering and high-strain deformation of an $Al_{0.1}$CrCoFeNi high-entropy alloy, Sci. Rep. 6 (1) (2016) 1–11.
[26] A. Sharma, Multi-Principal Element Alloys: Design, Properties and Heuristic Explorations, Iowa State University, 2018 Ph.D. thesis.
[27] S. Wang, K. Hou, H. Heinz, Accurate and compatible force fields for molecular oxygen, nitrogen, and hydrogen to simulate gases, electrolytes, and heterogeneous interfaces, J. Chem. Theory Comput. 17 (8) (2021) 5198–5213.
[28] Z. Rak, D.W. Brenner, First-principles investigation of diffusion and defect properties of Fe and Ni in Cr_2O_3, J. Appl. Phys. 123 (15) (2018) 155105.
[29] P. Berthod, Kinetics of high temperature oxidation and chromia volatilization for a binary Ni–Cr alloy, Oxid. Met. 64 (3) (2005) 235–252.
[30] A. Heuer, Oxygen and aluminum diffusion in α-Al_2O_3: how much do we really understand? J. Eur. Ceram. Soc. 28 (7) (2008) 1495–1507.
[31] M.J. Graham, J. Eldrige, D. Mitchell, R. Hussey, Anion transport in growing Cr_2O_3 scales, in: Materials Science Forum, vol. 43, Trans Tech Publ, 1989, pp. 207–242.
[32] T.M. Butler, M.L. Weaver, Oxidation behavior of arc melted AlCoCrFeNi multi-component high-entropy alloys, J. Alloys Compd. 674 (2016) 229–244.